Chinese Chemical Letters 36 (2025) 110457

Contents lists available at ScienceDirect

Chinese Chemical Letters

journal homepage: www.elsevier.com/locate/cclet

Recent progress on non-metallic carbon nitride for the photosynthesis of H_2O_2: Mechanism, modification and *in-situ* applications

Hao Lv[a], Zhi Li[a], Peng Yin[b,*], Ping Wan[c,*], Mingshan Zhu[a,*]

[a] College of Environment and Climate, Jinan University, Guangzhou 511443, China
[b] Jiading Branch of Shanghai General Hospital, Shanghai Jiao Tong University School of Medicine, Shanghai 201803, China
[c] Department of Liver Surgery, Ren Ji Hospital, Shanghai Jiao Tong University School of Medicine, Shanghai 200127, China

ARTICLE INFO

Article history:
Received 30 May 2024
Revised 3 September 2024
Accepted 12 September 2024
Available online 14 September 2024

Keywords:
Carbon nitride
Hydrogen peroxide
Photocatalysis
Applications

ABSTRACT

Photocatalytic hydrogen peroxide (H_2O_2) production has been considered as a promising strategy for H_2O_2 synthesis due to its environmentally friendly. Among various photocatalysts, carbon nitride-based materials are excellent candidates for H_2O_2 production because of their excellent visible-light response, low cost and high stability. In this review, we summarize in detail the research progress on the photocatalytic production of H_2O_2 by carbon nitride. First, we summarize the basic principles of photocatalysis and photocatalytic H_2O_2 production. Second, the classification and modification methods of carbon-nitride-based materials are discussed, including morphology modulation, noble metal loading, defect control, heterojunction regulation, molecular structure engineering and elemental doping. Finally, the different *in-situ* applications of H_2O_2 *via* photosynthesis were discussed, including disinfection and antibiotic resistant genes degradation, organic pollutants degradation, medical applications and fine chemical synthesis. This review brings great promise for *in-situ* H_2O_2 photosynthesis, which is expected to serve as a key component in future applications.

1. Introduction

Hydrogen peroxide (H_2O_2) serves as an environmentally friendly oxidizing agent and one of the most important chemicals for industrial application [1,2]. Presently, the industrial method to synthesis H_2O_2 always involves the anthraquinone process, which always depends on organic solvents and noble metal catalysts, bringing high energy consumption [3]. Another traditional method is the direct synthesis of H_2O_2 from H_2 and O_2 on Pd-based catalysts [4]. Nevertheless, this approach also exhibits numerous challenges, including the explosive properties of H_2/O_2 mixture and the decomposability of H_2O_2 in alkaline environment. Therefore, it is imperative to develop cost-effective, green and safe methods for H_2O_2 synthesis to tackle the energy and environmental challenges.

Photocatalysis has been considered as the most promising method to synthesize H_2O_2. Since Baur *et al.* reported that H_2O_2 was produced from glycerol and glucose using ZnO under light in 1927 [5], a large number of researchers [6–14] have been working on the photocatalytic H_2O_2 production. This process of photocatalytic H_2O_2 production involves utilizing light energy to activate a semiconductor material, which facilitates the reaction between O_2 and H_2O to generate H_2O_2. This method offers several advantages over traditional synthesis methods, including minimizing waste generation and reducing energy consumption.

Currently, among various photocatalytic materials for H_2O_2 production, non-metallic carbon nitride has garnered significant attention. In 2009, Wang *et al.* first reported that carbon nitride was capable of photocatalytic H_2 production [15]. This has sparked widespread exploration of carbon nitride within the field of photocatalysis [16–22]. Carbon nitride does not require any addition of metal ions, and demonstrates excellent chemical stability and large specific surface area, facilitating catalytic reactions. Furthermore, carbon nitride has special band positions, which are well-suited for oxygen reduction reaction (ORR) and water oxidation reaction (WOR) to produce H_2O_2.

Although there are many reviews on photocatalysis by carbon nitride, they always focused on H_2 production and CO_2 reduction. There is still a lack of a separate and detailed review on photocatalytic H_2O_2 production, especially with *in-situ* applications. Based on this, we herein summarize the relevant research on photocatalytic synthesis of H_2O_2 by carbon nitride. As shown in Fig. 1, it begins with the fundamental mechanisms of photocatalysis. Secondly, different modification methods for carbon nitride-based materials, including morphology tuning, noble metal loading, defect

* Corresponding authors.
E-mail addresses: randywsyghxs@hotmail.com (P. Yin), gufeng182@126.com (P. Wan), zhumingshan@jnu.edu.cn (M. Zhu).

https://doi.org/10.1016/j.cclet.2024.110457
1001-8417/

Fig. 1. Principle, clsssification, modification of carbon nitride-based catalysts for H_2O_2 photosynthesis and their *in-situ* applications.

control, heterojunction regulation, molecular structure engineering, and elements doping, are summarized. Finally, various *in-situ* applications of H_2O_2 photosynthesis are discussed, including disinfection and antibiotic resistant genes (ARGs) degradation, organic pollutants degradation, medical applications and fine chemical synthesis.

2. Principle

2.1. Photocatalytic principle of carbon nitride

Photocatalysis refers to the process of converting light energy into chemical energy for catalyzing chemical reactions under light irradiation [23,24]. With light irradiation, photocatalysts could absorb sufficient light energy, and then the photogenerated electrons (e^-) could be excited from valence band (VB) to conduction band (CB), while positively charged holes (h^+) remain in the VB. Then, e^- and h^+ migrate to the surface of the catalyst and participate in redox reactions. At the same time, photoinduced e^- and h^+ also undergoes bulk recombination and surface recombination, resulting the quenching of e^- and h^+ (Fig. 2a).

2.2. Principle of photocatalytic H_2O_2 production

The currently recognized mechanisms of photocatalytic H_2O_2 production mainly include ORR and WOR, where ORR occurs at CB, while WOR occurs at VB (Fig. 2b). In details, there are two main ways for ORR, including two-step one-electron ($1e^-$) process Eqs. 1–4, with a reduction potential of $E^0 = -0.33$ V and a one-step two-electron ($2e^-$) process (Eq. 5), with a reduction potential of $E^0 = +0.68$ V. Firstly, $1e^-$ ORR produces superoxide radical ($O_2^{\bullet -}$) (Eq. 1), which further reacts with H^+ to produce $HO_2^{\bullet -}$ (Eq. 2). Then, $HO_2^{\bullet -}$radical can be readily followed by another $1e^-$ reduction to produce HO_2^- anion (Eq. 3). Finally, HO_2^- reacts with H^+ to produce H_2O_2 (Eq. 4). In addition, a direct one-step $2e^-$ reduction to produce H_2O_2 involves the combination of O_2 and $2H^+$ and $2e^-$ (Eq. 5) [25,26].

$$O_2 + e^- \rightarrow O_2^{\bullet -} \quad (1)$$

$$O_2^{\bullet -} + H^+ \rightarrow HO_2^{\bullet -} \quad (2)$$

$$HO_2^{\bullet -} + e^- \rightarrow HO_2^- \quad (3)$$

$$HO_2^- + H^+ \rightarrow H_2O_2 \quad (4)$$

$$O_2 + 2H^+ + 2e^- \rightarrow H_2O_2 \quad (5)$$

The above reaction processes are main paths of H_2O_2 production. Besides, there are also some pathways by WOR [27–29]. WOR is achieved through that photogenerated h^+ reacts with H_2O to generate H_2O_2, including direct $2e^-$ WOR and $1e^-$ WOR. In detail, photoinduced h^+ directly oxidizes H_2O to H_2O_2 ($2e^-$ WOR) (Eq. 6) with an oxidation potential of $E^0 = +1.76$ V. In addition, h^+ first oxidizes hydroxide ions (OH^-) to generate hydroxyl radicals ($^{\bullet}OH$) (Eq. 7), and then indirectly generates H_2O_2 through the combination of $2^{\bullet}OH$ ($1e^-$ WOR) (Eq. 8). The oxidation potential require for this process is $E^0 = +1.99$ V [30].

$$2H_2O + 2h^+ \rightarrow H_2O_2 + 2H^+ \quad (6)$$

$$OH^- + h^+ \rightarrow {}^{\bullet}OH \quad (7)$$

$${}^{\bullet}OH + {}^{\bullet}OH \rightarrow H_2O_2 \quad (8)$$

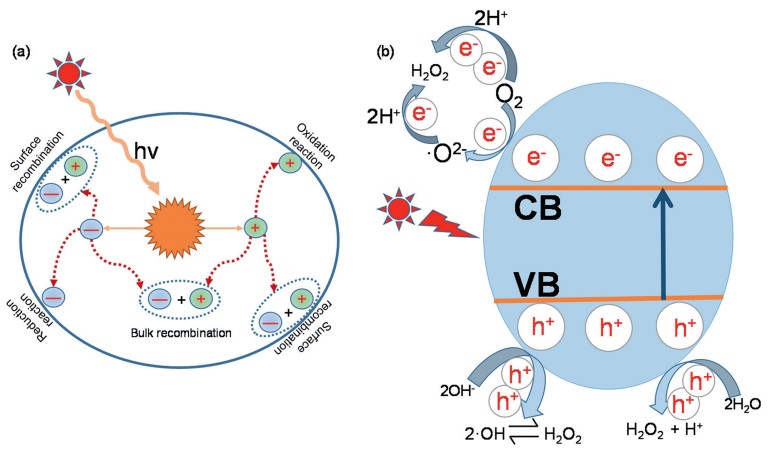

Fig. 2. (a) Photoexcitation and charge decay pathways in photocatalysts. (b) Schematic diagram of photocatalytic system for producing H_2O_2.

3. Classification of carbon nitride

Since C_3N_4-based carbon nitride was reported by Wang in 2009 [15], many researchers have devoted their attention to this kind of material. In addition to C_3N_4 with a carbon to nitrogen (C/N) ratio of 0.75, other carbon nitrides with different C/N ratios have been synthesized, including a class of carbon nitride with C/N < 0.75 (C_3N_5, C_3N_6, C_3N_7, *etc.*), and that with C/N > 0.75 (C_3N_3, $C_{3.6}N$, C_5N_2, *etc.*) (Fig. 3).

3.1. C/N=0.75

The most common carbon nitride is material with C/N = 0.75, corresponding to C_3N_4. C_3N_4 structure has several isomers, such as a-C_3N_4, b-C_3N_4, cubic-C_3N_4, *pseudo*-C_3N_4 and graphite-C_3N_4 (g-C_3N_4). Among these, g-C_3N_4 structure is the most stable isomer under environmental conditions and serves as the most commonly used photocatalyst [17,19]. The group of g-C_3N_4 mainly include triazine-based g-C_3N_4 and tri-*s*-triazine (heptazine)-based g-C_3N_4 [21].

Nowadays, lots of synthetic methods were developed to prepare g-C_3N_4 [18]. Wang *et al.* proposed a method for synthesizing g-C_3N_4 *via* putting cyanamide to temperatures ranging from 400 °C to 600 °C (ramp rate: 2.2 °C/min) for 4 h [15]. Besides, C_3N_4 could also be synthesized using melamine as a precursor [31–33]. Firstly, melamine was formed through polymerization and condensation, followed by rearrangement into tri-*s*-triazine based compounds at around 390 °C, further condensation into polymers, networks and potentially the final polymeric g-C_3N_4 at around 520 °C [33]. Other prevalent precursors included urea and dicyandiamide (DCD). For example, Li *et al.* synthesized g-C_3N_4 by thermal polymerization using these two precursors [34]. In detail, 10.0 g of urea and DCD powders were put in an Al_2O_3 crucible with a half-cover state. The mixture underwent heating in a muffle oven at a rate of 10 °C/min until reaching a certain temperature, which was maintained for 3 h to obtain g-C_3N_4.

3.2. C/N < 0.75

Carbon nitrogen with C/N < 0.75 are called N-rich carbon nitrides. This kind of carbon nitride usually exhibits higher photocatalytic activity due to its nitrogen functional groups, which provide many active sites [35–40]. The N-rich carbon nitrogen mainly include C_3N_5, C_3N_6 and C_3N_7.

For C_3N_5, Gillan *et al.* proposed a method for synthesizing this material *via* azide-based molecular precursors in 2000 [41]. Azide and triazine were selected as the precursors. The triazido-triazine was decomposed in a high-pressure steel reactor under 6 atm N_2 with a gradual heating to 185 °C and then it was maintained at this temperature for 24 h to produce C_3N_5. For C_3N_6, Talapaneni and co-workers reported a method to synthesize C_3N_6 at a low temperature to avoid traditional high-temperature process by using amino guanidine [39]. Besides, other C_3N_5 materials (MCN-4-x) were synthesized using SBA-15 as a hard template [39]. The N/C ratios of MCN-4-x samples gradually increased with the increase of initial mixing temperature. The synthesis of C_3N_7 was achieved by pyrolysis of 5-amino-1*H*-tetrazole (5-ATTZ) at 250 °C *via* nanotemplating approach [40]. The detailed steps were as follows: 3.14 g of 5-ATTZ was dispersed in 11.0 g of deionized H_2O at 50 °C, and then 1.0 g of KIT-6 was added. The suspension was mixed and heated in an oven at 100 °C for 6 h. The obtained sample was calcined at 250 °C under N_2 for 4 h. Then, KIT-6 crystals were removed with 5 wt% hydrofluoric acid and ethanol. Finally, C_3N_7 was obtained by drying at 100 °C for 12 h.

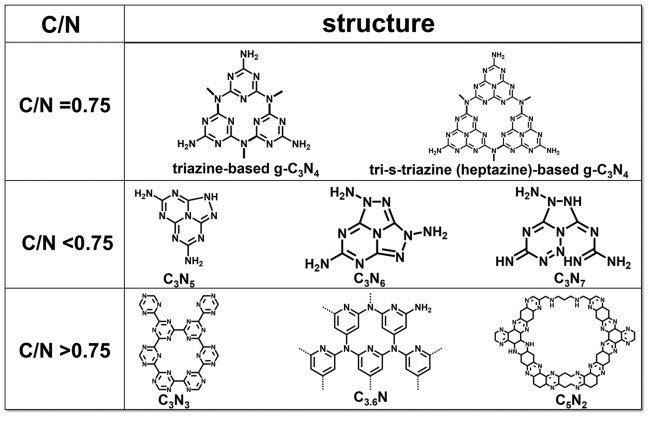

Fig. 3. Types of main carbon nitride.

3.3. C/N > 0.75

Carbon nitrogen with C/N > 0.75 is called C-rich carbon nitride, which always displays better conductivity and mechanical properties [42–45]. There are several techniques for synthesizing this kind of carbon nitride. For example, Kim *et al.* prepared the synthesis of N-deficient C_3N_3 and C_3N-based carbon nitrides from various single-molecule precursors [42]. They impregnated three precursors, including phosphomolybdic acid hydrate (PMA), dithioxoamide (DTO) and 5-ATTZ, into the KIT-6 porous hard template and then calcined them at high temperature to finally obtain C_3N_3 hybrid. Similarly, Feng and Li *et al.* synthesized C_3N_3 by using Ullmann reaction to achieve homocoupling of aryl halides [43]. They adopted cyanuric chloride ($C_3N_3Cl_3$) for polymerization within a sealed tube, utilizing copper foil as the substrate to obtain a layered C_3N_3 structure. Xu *et al.* also explored hexamethylenetetramine as a molecular precursor for the synthesis of $C_{3.6}N$ by thermal cleavage within a hard template (SBA-15) [44]. Ma *et al.* synthesized C_5N_2 through Schiff reaction using melamine and *p*-phthalaldehyde dyes as monomers, with an optimal molar ratio of 3:2 [45]. With the increase of synthesis time, the yield of insoluble solid product gradually increased, and C_5N_2 could be obtained after 5 days.

4. Carbon nitride modification

Carbon nitride has been demonstrated as a promising photocatalytic material for H_2O_2 production. However, the efficiency of carbon nitride in photocatalytic H_2O_2 production always depends on various factors. Therefore, we provide a comprehensive summary of modifications to improve the performance of carbon nitride, including morphology tuning, noble metal loading, defect control, heterojunction regulation, molecular structure engineering and elements doping, and some other modifications (Fig. 4).

4.1. Morphology tuning

Morphology tuning is a crucial technique that enables the manipulation of material morphology and structure, thereby influencing the performance of photocatalytic H_2O_2 production [25,46,47]. By controlling the synthesis conditions and incorporating template agents, surface modifiers, and other additives, it can be employed to achieve different morphology of carbon nitride [48]. For example, different carbon nitride with desired shapes, such as nanorods, nanosheets, and porous structures, can be obtained by adjusting the solution concentration or employing specific template agents.

Xu *et al.* synthesized uniformly porous carbon nitride nanotubes using a supramolecular self-assembly method [47]. They obtained uniform carbon nitride nanotubes (TCN-520) with 1–3 μm

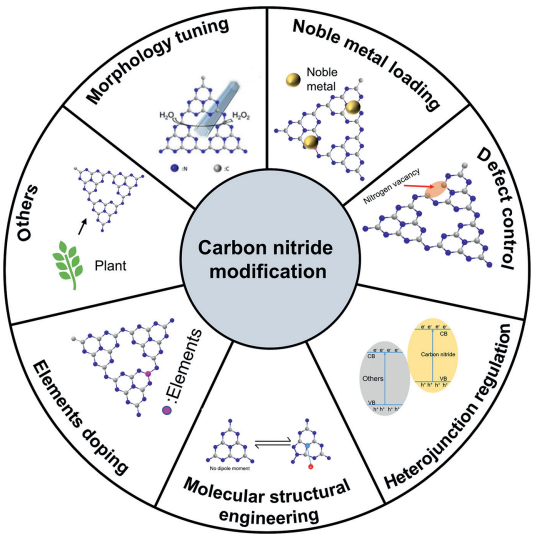

Fig. 4. Different modification methods of carbon nitride.

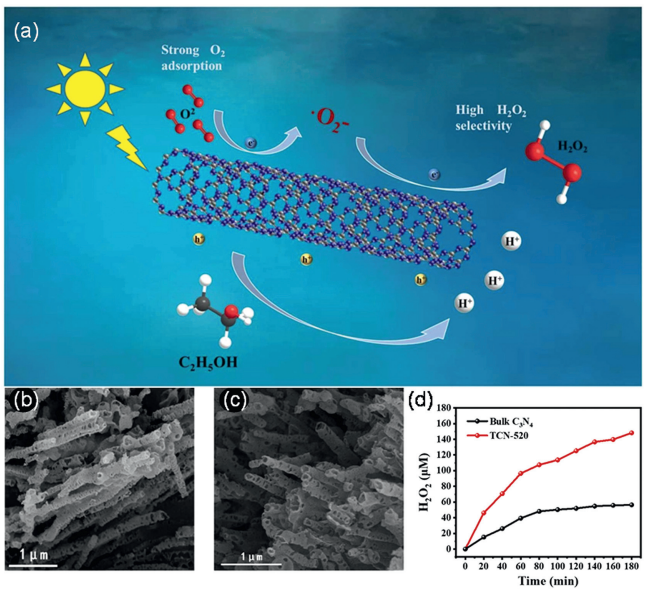

Fig. 5. (a) Mechanism of porous carbon nitride nanotube for H_2O_2 production; (b, c) TCN-520 transmission electron microscope (TEM) images of TCN-520. (d) Performance of TCN-520 and bulk C_3N_4 for H_2O_2 generation. Copied with permission [47]. Copyright 2023, Elsevier.

in length and a diameter of 10–20 nm *via* a calcination temperature of 520 °C. TCN-520 can generate H_2O_2 by the two-step $1e^-$ process (Fig. 5a). Additionally, the nanotube displayed a porous structure due to the gas released during the calcination process (Figs. 5b and c). TCN-520 exhibited a higher photocatalytic H_2O_2 yield than pristine bulk carbon nitride (Fig. 5d). The reasons could be attributed to that the nanotube structure had a large specific surface area, outstanding electron transport rate, O_2 adsorbing capability and high selectivity of $2e^-$ ORR.

In addition, three-dimensional (3D) structures also can enhance the performance of carbon nitride by regulating the surface area. For example, Li *et al.* synthesized ultrathin graphitic carbon nitride nanoplates with thickness of 1–3 nm for facilitating H_2O_2 production [25]. The ultrathin structure displays a larger surface area with a large number of active sites, and enhances redox capability compared to the pristine counterpart. The H_2O_2 production rate of obtained nanoplates was 43.07 μmol g^{-1} h^{-1}, which is about 4 times that of pristine g-C_3N_4.

4.2. Noble metal loading

The loading of noble metal mainly includes adding noble metal nanoparticles to the surface or interior of carbon nitride, aiming to boost the charge separation and enhance their photocatalytic performance. Noble metal nanoparticles generally serve as active sites in photocatalytic reactions to promote photogenerated carrier separation and selective reactions, thereby increasing the yield of H_2O_2 [49–52]. The selection of appropriate noble metal nanoparticles is crucial for increasing catalytic activity, as different metals show distinct electronic structures. By controlling the properties and interactions of noble metal nanoparticles, enhanced light absorption and carrier separation can be achieved, thereby increasing the yield of H_2O_2.

For example, Song *et al.* reported a method for loading and stabilizing gold nanoparticles on C_3N_4 substrates (Fig. 6a), which simultaneously enhanced the stability of the catalyst and the performance of H_2O_2 photosynthesis. The precursor was annealed for 2 h at 500 °C with N_2, exhibiting the best performance of 1320 μmol/L, which is 2.3 times that of pure C_3N_4. Among the various samples synthesized, Au/CN-100 had the largest production amount (Fig. 6b) [50].

Cai *et al.* prepared silver-decorated ultrathin g-C_3N_4 nanosheets (Ag@U-g-C_3N_4-NS) through post gas etching (PGE) technology (Fig. 6c). As shown in Fig. 6d, U-g-C_3N_4-NS produced the higher yield of H_2O_2 (0.414×10^{-6} mol L^{-1} min^{-1}) than that of B-g-C_3N_4 ($<0.03 \times 10^{-6}$ mol L^{-1} min^{-1}). The improved performance was due to that the large specific surface area of ultrathin g-C_3N_4 nanosheets (U-g-C_3N_4-NS) provided a large number of active sites [51], and Ag nanoparticles in Ag@U-g-C_3N_4-NS catalyst acted as an electronic bridge of photogenerated electron to form Schottky barriers, thereby reducing the charge recombination and improving hole utilization [52].

4.3. Defect control

Recently, defect control has been considered as an important way to improve photocatalytic efficiency [53–56]. The formation of defects can influence the electronic structure, energy band structure, and surface active sites of material, thereby promoting carriers separation and prolonging the lifetime of carriers. Moreover, the crystal structure and morphology of carbon nitride can also be changed by defect control. Lots of studies have clearly demonstrated the advantages of defect control in carbon nitride for boosting photocatalytic production of H_2O_2 [57–61].

Zhu's group synthesized reduced g-C_3N_4 with N vacancies by heat treatment with $NaBH_4$ under N_2 [58]. The N vacancies in C_3N_4 were formed by reduction treatment involving a cleavage reaction with the pyridine nitride of s-triazine-C_3N_4 (Fig. 7a). This led to the narrowing of energy bandgap to boost visible light-driven WOR capability [62,63]. In particular, N vacancies can promote the spatial separation of photogenerated e^- and h^+. As shown in Fig. 7b, R_{370}-CN could achieve photocatalytic production of H_2O_2 from pure H_2O and ambient atmosphere under visible light, reaching 170 μmol/L in 1 h. Zheng *et al.* prepared N-vacancy CN spheres (NVCNS) in H_2 plasma by low-temperature heating (Fig. 7c). Under visible light, NVCNS containing N vacancies could produce 250 μmol H_2O_2 in 2 h (Fig. 7d) [59]. In another investigation, Han *et al.* achieved the incorporation of two distinct N vacancy types into g-C_3N_4 through the pyrolysis of melamine under both Ar and NH_3, coupled with subsequent HNO_3 oxidation. It was worth noting that the pyrolysis atmosphere had a significant effect for producing N vacancies. The N vacancies in N groups (N_3C) and sp^2 hybrid N

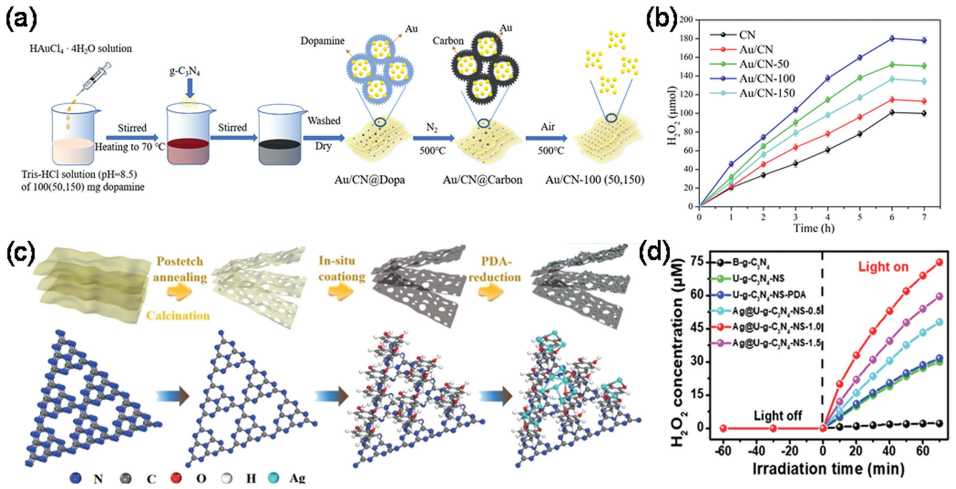

Fig. 6. (a) The preparation process for samples (the Au load is 2 wt% of carbon nitride). (b) Photocatalytic yield of H_2O_2 for different samples. Copied with permission [50]. Copyright 2022, Royal Society of Chemistry. (c) Stepwise representation of route to Ag NP–decorated ultrathin g-C_3N_4 nanosheets. (d) H_2O_2 production is accomplished by photocatalysis. Copied with permission [51]. Copyright 2019 Wiley-VCH.

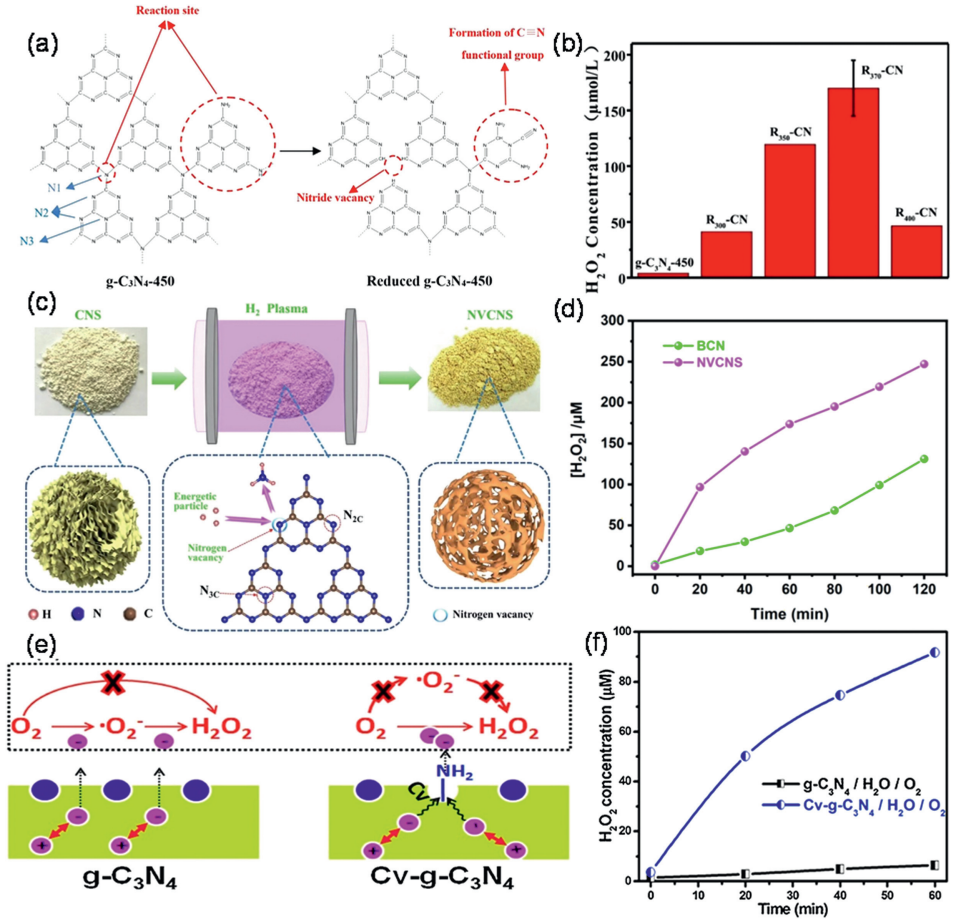

Fig. 7. (a) Possible N vacancies synthetic process. (b) Performance of different photocatalysts for H_2O_2 generation. Copied with permission [58]. Copyright 2018, Elsevier. (c) The schematics of H_2 plasma process of NVCNS. (d) Yield of photocatalytic production of H_2O_2 (>420 nm). Copied with permission [59]. Copyright 2022, Elsevier. (e) Mechanisms of H_2O_2 production with Cv-g-C_3N_4. (f) The concentration of H_2O_2 generated *via* g-C_3N_4 and Cv-g-C_3N_4. Copied with permission [61]. Copyright 2016, Elsevier.

atoms (N_2C) could be formed under NH_3 pyrolysis and Ar pyrolysis, respectively [60]. For carbon nitride, C vacancies building is another way for defect control. For example, Li *et al.* proposed a thermal annealing method under Ar atmosphere to generate C vacancies in g-C_3N_4 (Cv-g-C_3N_4) [61]. The results showed that g-C_3N_4 with C vacancies exhibited higher photocatalytic production of H_2O_2 compared to pure g-C_3N_4. The increased photocatalytic performances were attributed to extending visible light absorption and increasing charger separation with Cv-g-C_3N_4. Furthermore, the NH_3 groups surrounding carbon vacancies changed the H_2O_2 production pathway from two-step indirect reaction to one-step direct reaction, thereby accelerating the synthesis of H_2O_2 (Fig. 7e).

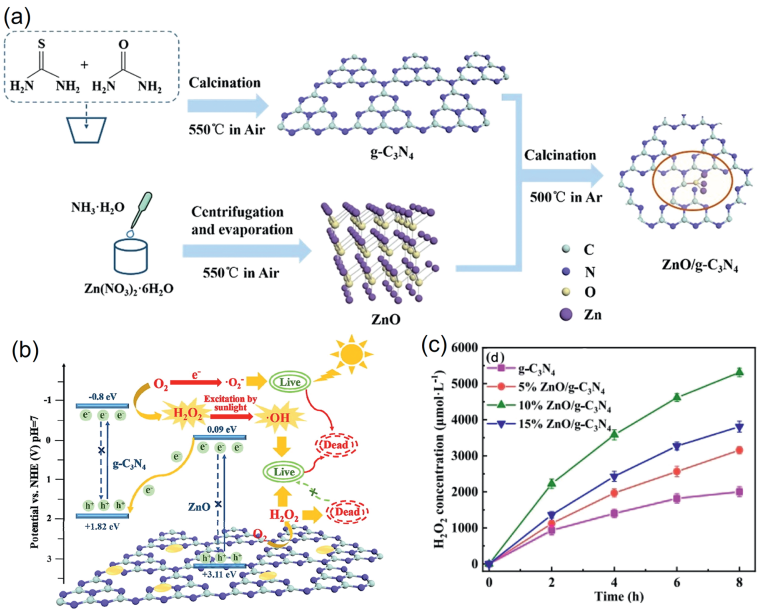

Fig. 8. (a) Synthetic process of ZnO/g-C_3N_4 heterojunction photocatalyst. (b) Mechanisms of H_2O_2 production and photocatalytic sterilization. (c) Performance of different catalysts for H_2O_2 generation. Copied with permission [66]. Copyright 2021, Elsevier.

As shown in Fig. 7f, the yield of Cv-g-C_3N_4 was 14 times that of g-C_3N_4.

4.4. Heterojunction regulation

Heterojunction regulation is an effective approach for regulating the production of H_2O_2 from carbon nitride. A built-in electric field can be generated in the interface between both different materials, thereby enhancing the catalytic activity and selectivity. Common control strategies include semiconductor heterojunctions [64], metal-semiconductor heterojunctions [65,66] and two-dimensional material composite heterojunctions [67]. These approaches can tune electron transport and interfacial interactions to enhance the efficiency of H_2O_2 generation [68].

For example, Geng *et al.* used a hydrothermal method to prepare ZnO/g-C_3N_4 heterojunction catalyst (Fig. 8a), which significantly improved the production of H_2O_2 [66]. The reaction mechanisms were shown in Fig. 8b. 10 wt% ZnO/g-C_3N_4 exhibited a H_2O_2 yield of 5312.45 μmol/L after 8 h, which was 2.65 times higher than that of pure g-C_3N_4 (Fig. 8c). The high performance was due to: (i) Enhancement of light-absorbing capacity by constructing a heterojunction between ZnO and g-C_3N_4 from ultraviolet to visible light; (ii) Separation of photogenerated e^- and h^+ at the interface between ZnO and g-C_3N_4; (iii) Facilitating electron transfer between ZnO and g-C_3N_4.

4.5. Molecular structural engineering

Charge recombination in the photocatalysts includes bulk recombination (BR) and surface recombination (SR). SR behavior usually takes tens of nanoseconds to occur, whereas BR often occurs within picoseconds. Therefore, the reduction of BR plays a vital role in improving the photocatalytic activity of carbon nitride. Utilizing structural engineering to enhance dipole field effects is an important strategy to promote directional bulk electron separation [69,70].

Li *et al.* reported a novel process with dipole field-driven spontaneous polarization in N-rich triazole-based carbon nitride (C_3N_5) to boost the photocatalytic synthesis of H_2O_2 [71]. The existence of dipole field facilitated redox reactions by influencing its electron cloud distribution. Fig. 9a illustrated the dipole field and its variations under external force. Density functional theory (DFT) revealed that C_3N_5 displayed a dipole moment, while C_3N_4 did not show any dipole moment (Fig. 9b). The significant dipole moment in C_3N_5 enabled the utilization of dipole field-induced spontaneous polarization to leverage photogenerated charge separation dynamics. The results showed that the H_2O_2 production rate of C_3N_5 was 3809.5 μmol g^{-1} h^{-1} (Fig. 9c), which was superior to the performance of pure g-C_3N_4. The reaction mechanism was shown in Fig. 9d. This straightforward technique address a critical need in facilitating the transfer of photoinduced carriers through the introduction of structural engineering induced dipole field.

4.6. Elements doping

Doping elements can determine the electronic structure, lattice configuration, and surface characteristics of carbon nitride, thereby realizing the regulation of catalytic performance [72,73]. By introducing elements, the electronic structure of material, additional active sites, and the electron transfer rate are improved. The metal doping including Cu or Fe, *etc.* can highly improve the catalytic activity of H_2O_2 [74–76]. In addition, non-metallic doping elements such as nitrogen, phosphorus, sulfur, and selenium also tune the selectivity of carbon nitride to synthesis H_2O_2 [27,77,78].

For example, Li *et al.* doped Cu or Fe into C_3N_4 by using thermal polymerization. The H_2O_2 yield of Cu- and Fe-doped C_3N_4 photocatalysts was 24.5 and 13.7 μmol/L, respectively, which was much higher than the original C_3N_4 [74]. There are also corresponding examples for non-metal doped carbon nitride. Cao *et al.* obtained phosphorus-doped porous carbon nitride (CPN) as a metal-free photocatalyst by uniformly mixing and calcining urea and phosphorus chloride trimer through hydrothermal method. The morphology of CPN were shown in Figs. 10a and b, with a porous structure. The elemental mappings of CPN confirmed the presence of C, N and P (Figs. 10c-e). A dual-channel pathway involving both WOR and ORR was observed, achieving a remarkable H_2O_2 yield of 1968 μmol g^{-1} h^{-1} without any sacrificial agents and co-catalysts, under ambient conditions (Fig. 10f) [27].

Besides, dual elements co-doping is also developed to modify carbon nitride [79–81]. Liu *et al.* designed oxypotassium double

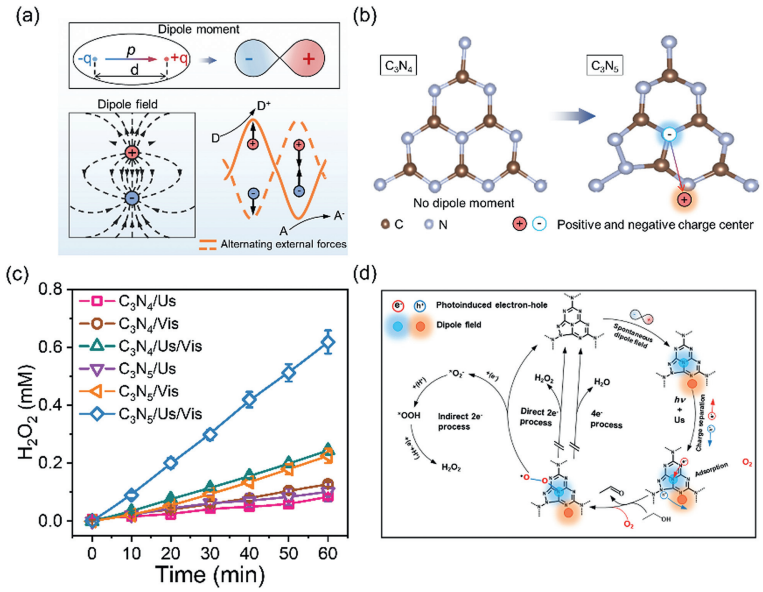

Fig. 9. (a) Dipole moment and the distribution of electron clouds. (b) The structural units of C_3N_4 and C_3N_5. (c) Time profiles of H_2O_2 production by photocatalysis of C_3N_5 and C_3N_4 under different reaction conditions. (d) Possible mechanisms of H_2O_2 generation. Copied with permission [71]. Copyright 2023, Springer Nature.

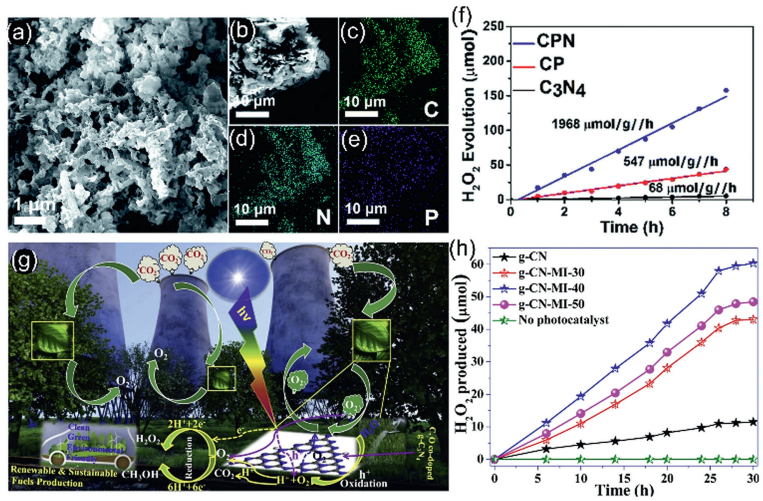

Fig. 10. (a, b) scanning electron microscope (SEM) images of CPN. (c–e) The corresponding energy dispersive spectrometer (EDS) elemental mappings of constituent elements for CPN. (f) Time profiles of photocatalytic H_2O_2 production with different catalysts. Copied with permission [27]. Copyright 2020, Royal Society of Chemistry. (g) Mechanisms of CO_2 reduction and H_2O_2 production process. (h) Photocatalytic H_2O_2 production of various catalyst. Copied with permission [81]. Copyright 2019, Elsevier.

heteroatom polymerized carbon nitride (O/K-CN) [79]. The addition of heteroatoms not only improved the adsorption of O_2 and the carrier separation, but also promoted the production of $^{\bullet}OOH$. The rate of H_2O_2 generation was as high as 309.44 μmol L^{-1} h^{-1} mg^{-1}, surpassing the other C_3N_4-based photocatalysts. Che *et al.* prepared K and I co-doped polymer g-C_3N_5 (g-C_3N_5-K, I) by calcining a mixture of 3-amino-1,2,4-triazole and KI [80]. The photocatalytic H_2O_2 production rate over g-C_3N_5-K, I (2933.4 μmol L^{-1} h^{-1}) exceeded that of g-C_3N_5. This high activity was attributed to the introduction of co-doping of K and I, which notably enhanced O_2 adsorption capacity and 2e- ORR selectivity. Subhajyoti *et al.* synthesized O and C co-doped g-C_3N_4 by thermal polymerization [81]. The obtained photocatalyst could be used for both CO_2 photoreduction and production of H_2O_2 from dissolved O_2 in H_2O (Fig. 10g). As shown in Fig. 10h, all samples could produce H_2O_2 for a long time, and the performance of g-CN-MI-40 was much higher than that of pure C_3N_4. After 30 h of reaction, the yield of CN-MI-40 was approximately 6 times that of pure C_3N_4 [81].

4.7. Others

The surface characteristics and energy band structure of g-C_3N_4 can be regulated by integrating natural dead leaves into urea polymerization process. For example, Li *et al.* utilized natural dead leaves as both a morphology regulator and a carbon source to prepare porous carbon-doped g-C_3N_4 (PCCN) to obtain C_3N_4 nanopores (Fig. 11a) [82]. The yield of H_2O_2 was 37.44 μmol/L under visible light, which was higher than pure C_3N_4 (Fig. 11b).

Besides, single-atom doping is also an effective mean to regulate the properties of materials [30,83]. It is mainly realized through the combination of selected atoms and other functional groups. These can influence the electronic structure, chemical activity and optical properties of catalyst. For example, Ren *et al.* prepared a Mn single atom anchored graphitic carbon nitride (g-C_3N_4) with arylamino group (Fig. 11c). It could directly produce H_2O_2 from seawater (Fig. 11d), and the yield of H_2O_2 was 2230 μmol/L (Fig. 11e) [30].

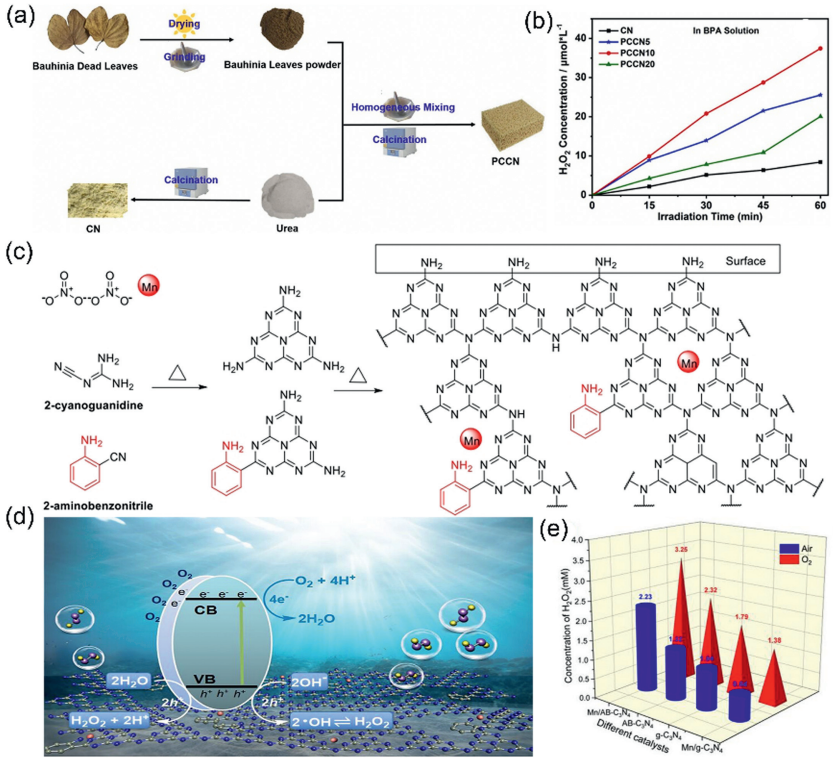

Fig. 11. (a) The synthesis process of PCCN sample. (b) Time profiles of photocatalytic H_2O_2 production with different catalysts. Copied with permission [82]. Copyright 2022, Elsevier. (c) The synthesis process of Mn/AB-C_3N_4. (d) Possible reaction mechanisms of H_2O_2 production. (e) Photocatalytic H_2O_2 production using different modified g-C_3N_4 catalysts. Copied with permission [30]. Copyright 2023, American Chemical Society.

5. *In-situ* applications

H_2O_2 is a green and clean resource, which displays wide application in energy and environmental processes, such as disinfection and antibiotic resistant genes degradation, organic pollutants degradation, medical applications, and fine chemical synthesis.

5.1. Disinfection and antibiotic resistant genes degradation

Compared to traditional disinfection methods, H_2O_2 presents excellent environmental friendliness. In a photocatalytic H_2O_2 system, H_2O_2 can be produced on-site and on-demand, presenting a more convenient and safer alternative to traditional disinfection methods. Consequently, the *in-situ* utilization of H_2O_2 generated through carbon nitride photocatalysis for disinfection and sterilization has garnered significant attention for researchers [34,66,71].

It is commonly believed that photocatalytic disinfection is carried out by reactive oxygen species (ROS), which can attack bacteria, thereby disrupting their physiological structure, antioxidant enzyme system, and respiratory system [84]. Geng *et al.* prepared ZnO/g-C_3N_4 catalyst for H_2O_2 generation and *in-situ* sterilization of natural water under sunlight irradiation [66]. The sterilization rate reached 97.4% after 60 min with 10% ZnO/g-C_3N_4. Similarly, Li *et al.* used C_3N_5 to produce H_2O_2 to disinfect *E. coli* at different initial concentrations and achieved 100% inhibition rate at 60 min (Fig. 12a) [71]. In another work, they also constructed an *in-situ* self-photo-Fenton reaction system for the removal of oxytetracycline (OTC) contaminants and antibiotic resistance genes (ARGs) using C_3N_4. The results showed good antimicrobial properties (Figs. 12b and c) [34].

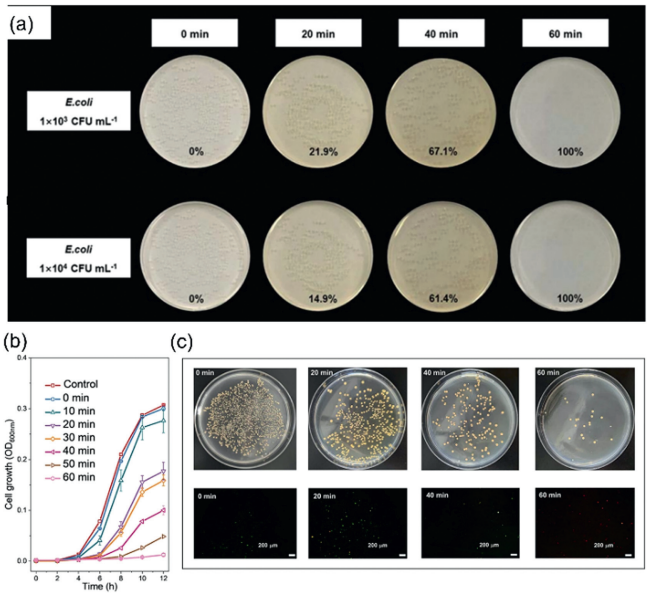

Fig. 12. (a) The disinfection rate of *E. coli.* Copied with permission [71]. Copyright 2023, Springer Nature. (b) MRSA growth curves. (c) Plate incubated with LB medium and live/dead staining (merge). Copied with permission [34]. Copyright 2024, Elsevier.

5.2. Organic pollutants degradation

The degradation of various organic pollutants by H_2O_2 has been recognized as an effective strategy, and many related works have been carried out [29,82,85–89]. However, the degradation, particularly mineralization, of organic contaminants requires a higher oxidative capacity. The *in-situ* Fenton reaction can address the above challenges. Consequently, many researchers have explored *in-situ* Fenton or *in-situ* Fenton-like reactions to enhance degradation efficiency.

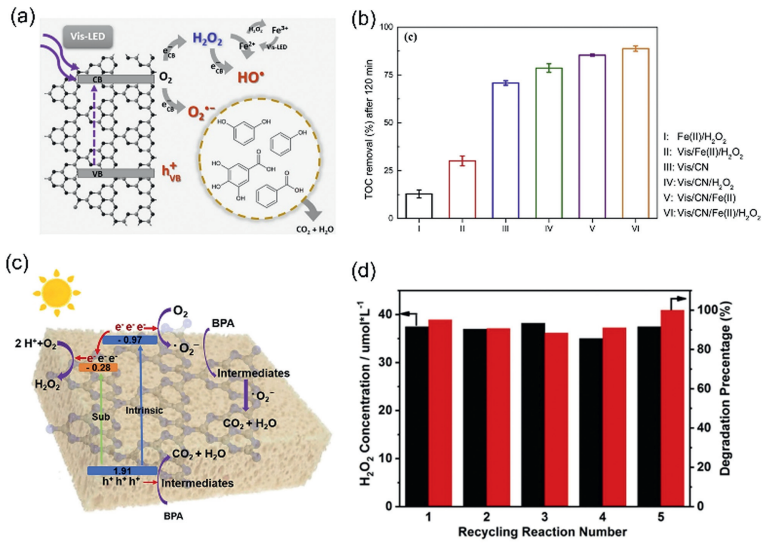

Fig. 13. (a) *In-situ* self-Fenton mechanism diagram. (b) Removal of TOC in different reaction environments. Copied with permission [89]. Copyright 2020, Elsevier. (c) Photogenerated electron-hole pair transfer pathway and the mechanism of simultaneous degradation of BPA by H_2O_2 generation. (d) Photocatalytic generation of H_2O_2 and simultaneous degradation of BPA in a cyclic experiment. Copied with permission [82]. Copyright 2022, Elsevier.

For example, Torres-Pinto *et al.* constructed an *in-situ* self-Fenton system using prepared g-C_3N_4 (Fig. 13a). This system showed the high mineralization rate with pure photocatalytic system, which was five times higher than that of conventional Fenton system. After the addition of Fe^{2+}, the mineralization rate of *in-situ* self-Fenton system increased by 20% (Fig. 13b) [89]. This result demonstrated the potential of carbon nitride used for *in-situ* self-Fenton systems for the degradation of organic pollutants. Li *et al.* also attempted to degrade BPA *via* an *in-situ* self-Fenton system (Fig. 13c). These results showed a good degradation efficiency for five cycles, demonstrating the excellent stability of prepared g-C_3N_4 (Fig. 13d) [82].

5.3. Medical applications

Due to H_2O_2 is a natural metabolite of many organisms, it has a wide range of applications in biomedicine [90]. H_2O_2 decomposes directly into H_2O and O_2, leaving no toxic residues or harmful by-products, posing harmlessness to human health and the environment. Thus, researchers begin to extend photocatalytic H_2O_2 production with carbon nitride to medicine field including sensing and cancer therapy [45,91–94].

For example, the degradation of H_2O_2 can alleviate O_2 deprivation in the hypoxic tumor microenvironment, thus improving the effectiveness of photodynamic therapy (PDT) [94]. Based on this, Ma *et al.* reported C_5N_2 photocatalyst for the selective and non-sacrificial generation of H_2O_2 in both normoxic and anoxic systems [45]. Due to the reinforcement of delocalization of π-electrons by linkers in C_5N_2, the side H_2 evolution was thermodynamically eliminated, while WOR was kinetically promoted (Fig. 14a). The results showed that C_5N_2 had excellent performance of photocatalytic H_2O_2 production (Figs. 14b and c), and also led to fairly significant cell death in both normoxic and hypoxic cellular environments (Fig. 14d). Based on this, they then developed a C_5N_2-based $^{\bullet}OH$ generator and fluorescent agent for photodynamic hypoxic tumor therapy (Fig. 14e).

5.4. Fine chemical synthesis

Photocatalytic H_2O_2 production can also be used for organic chemical synthesis. Moreover, this approach is of great significance to the current energy and environmental challenges, as it allows the oxidation reaction to be carried out under mild conditions, avoiding the environmental pollution and waste treatment problems associated with strong oxidizing agents.

Up to now, researchers are directing their attention towards *in-situ* photocatalytic H_2O_2 production for fine chemical synthesis [3,95–98]. For example, a tandem system for *in-situ* photocatalytic H_2O_2 generation and propylene epoxidation was constructed by Zhang *et al.* (Fig. 15a). Carbon nitride with N_3C vacancies was first synthesized with the synergistic effect of Ar pyrolysis and precursors self-assembled at the supramolecular level. The results showed that prepared catalyst had excellent photocatalytic H_2O_2 performance (5775 μmol g^{-1} h^{-1}) (Fig. 15b), and the efficiency of synthesized propylene oxide (PO) was 5515 μmol g^{-1} h^{-1} with 99.1% selectivity (Fig. 15c) [98].

6. Summary and outlook

Photocatalytic H_2O_2 production has attracted widespread attention and has become a hot research topic. In this review, we firstly discuss the basic principles of photocatalysis and photocatalytic H_2O_2 production. Second, we briefly introduce the main current types of carbon nitrides and highlight different modification methods of carbon nitride, including morphology tuning, noble metal loading, defect control, heterojunction regulation, molecular structure engineering, and elements doping, *etc.* Finally, a wide range of *in-situ* applications for photocatalytic H_2O_2 production are displayed, including disinfection and antibiotic resistant genes degradation, organic pollutants degradation, medical applications, and fine chemical synthesis. It is important to emphasize here that the concentration of H_2O_2 by photocatalytic production is hard to meet industrial need. However, the miniaturization and rapidity of photocatalytic system easily make it a key component *in-situ* practical applications with small-dose.

Although some promising results have been achieved, the photocatalytic production of H_2O_2 from carbon nitride is still in its infancy. At present, the H_2O_2 yield of carbon nitride with photocatalysis is still relatively low, and there are still a lot of gaps to meet the requirements of industrial applications. Current main difficulties mainly include narrow light absorption range, low photoelectric conversion efficiency and design of new photocatalytic systems. Therefore, future effort should focus on the following aspects:

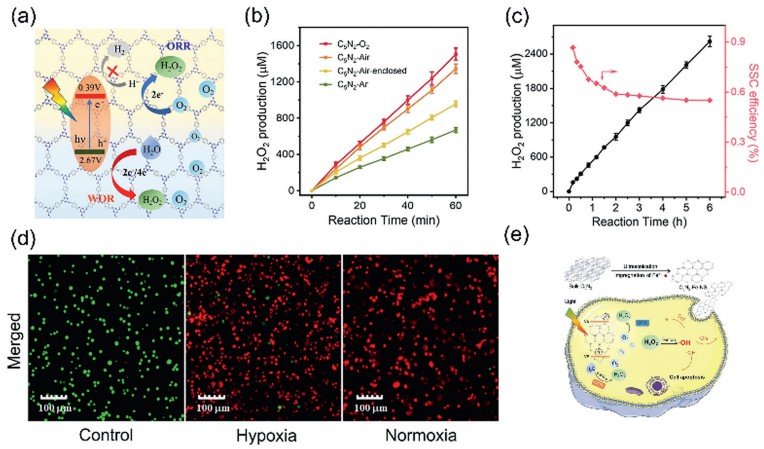

Fig. 14. (a) Mechanism of photocatalytic production of H_2O_2 by C_5N_2. (b) Time profiles of photocatalytic H_2O_2 production with different catalysts. (c) H_2O_2 production for long time and solar-to-chemical conversion (SCC) efficiency. (d) Live/dead double staining of C_5N_2−Fe−NS-treated 4T1 cells under light with FDA (green, live cells) and PI (red, dead cells). (e) Tumor therapy processes. Copied with permission [45]. Copyright 2022, Wiley-VCH.

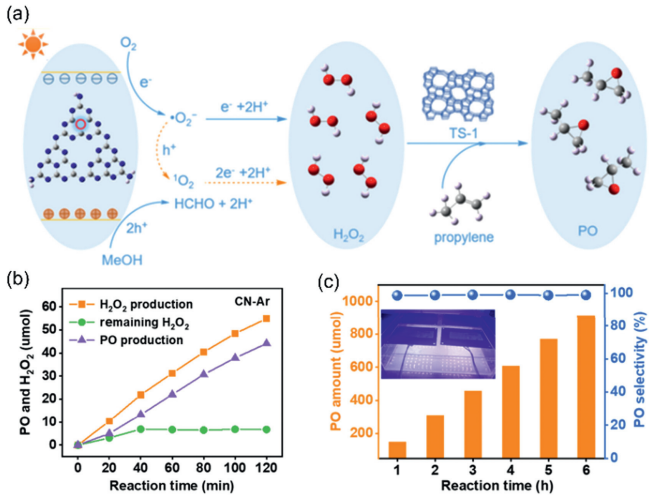

Fig. 15. (a) Mechanism diagram of *in-situ* photocatalytic H_2O_2 production and propylene epoxidation. (b) H_2O_2 production, PO production, and remaining H_2O_2 during the reactions. (c) Productivity and selectivity of PO. Copied with permission [98]. Copyright 2023, American Chemical Society.

(i) To improve the response range of carbon nitride to visible light. We should continue to broaden the absorption of materials into the visible and near-infrared regions through the development of new materials and material modification methods.

(ii) To design new photocatalyst forms. Currently, the mainstream photocatalyst form is powders. We should optimize these with immobilization methods by preparing membranes, sponges, aerogels and photoelectrodes, *etc.*

(iii) To design new photocatalytic systems. The current laboratory catalytic reaction system mainly depends on simple glass instruments. Therefore, we should design suitable *in-situ* photocatalytic reaction system in series and parallel connections under different catalytic scenarios and practical application scenarios.

Declaration of competing interest

The authors declare that they have no known competing financial interests or personal relationships that could have appeared to influence the work reported in this paper.

CRediT authorship contribution statement

Hao Lv: Writing – original draft, Data curation. **Zhi Li:** Writing – review & editing. **Peng Yin:** Writing – review & editing, Conceptualization. **Ping Wan:** Writing – review & editing, Conceptualization. **Mingshan Zhu:** Writing – review & editing, Resources, Project administration, Funding acquisition, Conceptualization.

Acknowledgment

This work has been supported by the National Key Research and Development Program of China (No. 2023YFC3705901).

References

[1] X. Wang, J. Jing, M. Zhou, R. Dewil, Chin. Chem. Lett. 34 (2023) 107621.
[2] K.P. Bryliakov, Chem. Rev. 117 (2017) 11406–11459.
[3] H. Zhao, Q. Jin, M.A. Khan, et al., Chem. Catal. 2 (2022) 1720–1733.
[4] R. Ciriminna, L. Albanese, F. Meneguzzo, M. Pagliaro, ChemSusChem 9 (2016) 3374–3381.
[5] E. Baur, C. Neuweiler, Helv. Chim. Acta 10 (1927) 901–907.
[6] Y. Zhao, P. Zhang, Z. Yang, et al., Nat. Commun. 12 (2021) 3701.
[7] S. Yan, Y. Li, X. Yang, et al., Adv. Mater. 36 (2024) 2307967.
[8] J. Ma, X. Peng, Z. Zhou, Y. Shen, Y. Zhang, Chin. Chem. Lett. 34 (2023) 108784.
[9] H. Hou, X. Zeng, X. Zhang, Angew. Chem. Int. Ed. 59 (2020) 17356–17376.
[10] L. Wang, J. Zhang, Y. Zhang, et al., Small 18 (2022) 2104561.
[11] S. Qu, H. Wu, Y.H. Ng, Adv. Energy Mater. 13 (2023) 2301047.
[12] J. Yang, X. Zeng, M. Tebyetekerwa, et al., Adv. Energy Mater. 14 (2024) 2400740.
[13] Z. Yong, T. Ma, Angew. Chem. Int. Ed. 62 (2023) e202308980.
[14] C. Yang, B. Cheng, J. Xu, J. Yu, S. Cao, EnergyChem 6 (2023) 100116.
[15] X. Wang, K. Maeda, A. Thomas, et al., Nat. Mater. 8 (2009) 76–80.
[16] T. Banerjee, F. Podjaski, J. Kröger, B.P. Biswal, B.V. Lotsch, Nat. Rev. Mater. 6 (2021) 168–190.
[17] S. Cao, J. Low, J. Yu, M. Jaroniec, Adv. Mater. 27 (2015) 2150–2176.
[18] L. Lin, Z. Yu, X. Wang, Angew. Chem. Int. Ed. 58 (2019) 6225–6236.
[19] Y. Zheng, L. Lin, B. Wang, X. Wang, Angew. Chem. Int. Ed. 54 (2015) 12868–12884.
[20] N.P. Dharmarajan, D. Vidyasagar, et al., Adv. Mater. 36 (2024) 2306895.
[21] W.J. Ong, L.L. Tan, Y.H. Ng, S.T. Yong, S.P. Chai, Chem. Rev. 116 (2016) 7159–7329.
[22] H. Li, B. Cheng, J. Xu, J. Yu, S. Cao, EES Catal. 2 (2024) 411–447.
[23] X. Wang, F. Wang, Y. Sang, H. Liu, Adv. Energy Mater. 7 (2017) 1700473.
[24] X. Du, H. Zhang, T. Yao, et al., Surf. Interfaces 48 (2024) 104283.
[25] W. Liu, C. Song, M. Kou, et al., Chem. Eng. J. 425 (2021) 130615.
[26] X. Xu, Y. Sui, W. Chen, et al., Appl. Catal. B: Environ. 341 (2023) 123271.
[27] J. Cao, H. Wang, Y. Zhao, et al., J. Mater. Chem. A 8 (2020) 3701–3707.
[28] H. Liang, A. Wang, R. Cheng, et al., Small 19 (2023) 2303813.
[29] Y.X. Ye, C. Wen, J. Pan, et al., Appl. Catal. B: Environ. 285 (2021) 119726.
[30] P. Ren, T. Zhang, N. Jain, et al., J. Am. Chem. Soc. 145 (2023) 16584–16596.
[31] X. Li, J. Zhang, L. Shen, et al., Appl. Phys. A 94 (2009) 387–392.
[32] Q. Liang, B. Shao, S. Tong, et al., Chem. Eng. J. 405 (2021) 126951.
[33] A. Thomas, A. Fischer, F. Goettmann, et al., J. Mater. Chem. 18 (2008) 4893–4908.
[34] Z. Li, H. Lv, K. Tong, et al., Appl. Catal. B: Environ. Energy 345 (2024) 123690.

[35] L. Huang, Z. Liu, W. Chen, D. Cao, A. Zheng, J. Mater. Chem. A 6 (2018) 7168–7174.
[36] P. Kumar, E. Vahidzadeh, U.K. Thakur, et al., J. Am. Chem. Soc. 141 (2019) 5415–5436.
[37] C. Liu, J. Zhang, W. Wang, L. Chen, M. Zhu, Surf. Interfaces 42 (2023) 103491.
[38] Y. Wang, T.N. Pham, Y. Tian, Y. Morikawa, L. Yan, J. Alloy. Compd. 585 (2021) 740–749.
[39] S.N. Talapaneni, G.P. Mane, A. Mano, et al., ChemSusChem 5 (2012) 700–708.
[40] I.Y. Kim, S. Kim, S. Premkumar, et al., Small 16 (2020) 1903572.
[41] E.G. Gillan, Chem. Mater. 12 (2000) 3906–3912.
[42] S. Kim, W. Cha, K. Ramadass, et al., Chem. Asian J. 15 (2020) 1863–1868.
[43] J. Feng, M. Li, Adv. Mater. 30 (2020) 2001502.
[44] J. Xu, T. Chen, X. Wang, B. Xue, Y.X. Li, Catal. Sci. Technol. 4 (2014) 2126–2133.
[45] J. Ma, X. Peng, Z. Zhou, et al., Angew. Chem. Int. Ed. 61 (2022) e202210856.
[46] Y. Cao, G. Zhou, X. Chen, et al., J. Mater. Chem. A 8 (2020) 124–137.
[47] Y. Song, C. Zhou, Z. Zheng, et al., J. Alloy. Compd. 934 (2023) 167901.
[48] J. Hwang, A. Ejsmont, R. Freund, et al., Chem. Soc. Rev. 49 (2020) 3348–3422.
[49] W. Yu, C. Hu, L. Bai, et al., Nano Energy 104 (2022) 107906.
[50] M. Song, H. Shao, Y. Chen, et al., Phys. Chem. Chem. Phys. 24 (2022) 29557–29569.
[51] J. Cai, J. Huang, S. Wang, et al., Adv. Mater. 31 (2019) 1806314.
[52] A. Murali, P.K. Sarswat, J.P.L. Perez, M.L. Free, Colloids Surfaces A 595 (2020) 124684.
[53] S. Bai, N. Zhang, C. Gao, Y. Xiong, Nano Energy 53 (2018) 296–336.
[54] D. Maarisetty, S.S. Baral, J. Mater. Chem. A 8 (2020) 18560–18604.
[55] J. Xiong, J. Di, J. Xia, W. Zhu, H. Li, Adv. Funct. Mater. 28 (2018) 1801983.
[56] N. Zhang, C. Gao, Y. Xiong, J. Energy Chem. 37 (2019) 43–57.
[57] Z. Zhang, Y. Zheng, H. Xie, et al., J. Alloy. Compd. 904 (2022) 164028.
[58] Z. Zhu, H. Pan, M. Murugananthan, J. Gong, Y. Zhang, Appl. Catal. B: Environ. 232 (2018) 19–25.
[59] Y. Zheng, Y. Luo, Q. Ruan, et al., J. Colloid Interf. Sci. 609 (2022) 75–85.
[60] Y. Zhu, X. Liu, H. Liu, et al., SusMat 2 (2022) 617–629.
[61] S. Li, G. Dong, R. Hailili, et al., Appl. Catal. B: Environ. 190 (2016) 26–35.
[62] S. Wang, J. Zhang, B. Li, H. Sun, S. Wang, Energy Fuels 35 (2021) 6504–6526.
[63] Q. Zhang, X. Chen, Z. Yang, et al., ACS Appl. Mater. Interfaces 14 (2022) 3970–3979.
[64] H. Wang, L. Zhang, Z. Chen, et al., Chem. Soc. Rev. 43 (2014) 5234–5244.
[65] S. Tan, A. Argondizzo, J. Ren, et al., Nat. Photonics 11 (2017) 806–812.
[66] X. Geng, L. Wang, L. Zhang, et al., Chem. Eng. J. 420 (2021) 129722.
[67] J. Low, S. Cao, J. Yu, S. Wageh, Chem. Commun. 50 (2014) 10768–10777.
[68] Y. Yang, Z. Zeng, G. Zeng, et al., Appl. Catal. B: Environ. 258 (2019) 117956.
[69] Z. Liu, C. Zhang, L. Liu, et al., Adv. Mater. 33 (2021) 2104099.
[70] Y. Zhang, Y. Luo, Y. Zhang, et al., Nature 531 (2016) 623–627.
[71] Z. Li, Y. Zhou, Y. Zhou, et al., Nat. Commun. 14 (2023) 5742.
[72] J. Chen, S. Fang, Q. Shen, et al., Catalysts 12 (2022) 962.
[73] E. Gaggero, W. Cai, P. Calza, T. Ohno, Surf. Interfaces 48 (2024) 104143.
[74] Z. Li, C. Kong, G. Lu, J. Phys. Chem. C 120 (2016) 56–63.
[75] S. Le, T. Jiang, Q. Zhao, et al., RSC Adv. 6 (2016) 38811–38819.
[76] S. Tonda, S. Kumar, S. Kandula, V. Shanker, J. Mater. Chem. A 2 (2014) 6772–6780.
[77] L. Xue, H. Sun, Q. Wu, W. Yao, J. Colloid Interf. Sci. 615 (2022) 87–94.
[78] D. Chen, C. Ma, Q. Zhang, et al., Surf. Interfaces 52 (2024) 104886.
[79] W. Liu, P. Wang, J. Chen, et al., Adv. Funct. Mater. 32 (2022) 2205119.
[80] H. Che, J. Wang, X. Gao, et al., J. Colloid Interf. Sci. 627 (2022) 739–748.
[81] S. Samanta, R. Yadav, A. Kumar, A.K. Sinha, R. Srivastava, Appl. Catal. B: Environ. 259 (2019) 118054.
[82] T. Li, X. Zhang, C. Hu, et al., J. Environ. Chem. Eng. 10 (2022) 107116.
[83] H. Li, B. Zhu, B. Cheng, et al., J. Mater. Sci. Technol. 161 (2023) 192–200.
[84] H. Zhong, X. Ji, C. Yang, et al., ACS Catal. 14 (2024) 6272–6291.
[85] Z. Li, Y. Chen, Y. Guo, et al., Appl. Surf. Sci. 598 (2022) 153866.
[86] Y. Chu, X. Zheng, J. Fan, Chem. Eng. J. 431 (2022) 134020.
[87] Q. Xu, J. Wu, Y. Qian, et al., ACS Appl. Mater. Interfaces 16 (2024) 784–794.
[88] S. Tian, Y. Yin, M. Liu, et al., Sep. Purif. Technol. 318 (2023) 124016.
[89] A. Torres-Pinto, M.J. Sampaio, J. Teixo, et al., J. Water Process Eng. 37 (2020) 101467.
[90] M. Dewaele, H. Maes, P. Agostinis, Autophagy 6 (2010) 838–854.
[91] Y. Fan, X. Gan, H. Zhao, et al., Chem. Eng. J. 427 (2022) 131572.
[92] M. Ye, C. Yang, Y. Sun, et al., ACS Appl. Nano Mater. 5 (2022) 10922–10932.
[93] G. Yang, Y. Chen, R. Shi, et al., Molecules 28 (2023) 3736.
[94] J. Kim, H.Y. Kim, S.Y. Song, et al., ACS Nano 13 (2019) 3206–3217.
[95] J.-J. Zhang, J.-M. Ge, H.-H. Wang, et al., ChemCatChem 8 (2016) 3441–3445.
[96] B.-H. Min, M.B. Ansari, Y.H. Mo, S.E. Park, Catal. Today 204 (2013) 156–163.
[97] Y. Wang, H. Li, J. Yao, X. Wang, M. Antonietti, Chem. Sci. 2 (2011) 446–450.
[98] Q. Zhang, L. Li, Q. Zhou, et al., ACS Catal. 13 (2023) 13101–13110.